Instability of the perfect subgrid model in implicit-filtering large eddy simulation of geostrophic turbulence

B. T. Nadiga* and D. Livescu†
LANL, Los Alamos, New Mexico 87545, USA

(Received 31 October 2006; revised manuscript received 24 January 2007; published 6 April 2007)

We demonstrate, in the context of implicit-filtering large eddy simulations (LESs) of geostrophic turbulence, that while the attractor of a well-resolved statistically stationary turbulent flow can be reached in a coarsely resolved LES that is forced by the subgrid scale (SGS) terms diagnosed from the well-resolved computation, the attractor is generically unstable: the coarsely resolved LES system forced by the diagnosed SGS eddy terms has multiple attractors. This points to the importance of interpreting the diagnosed SGS forcing terms in a well-resolved computation or experiment from a combined physical-numerical point of view rather than from a purely physical point of view.

DOI: 10.1103/PhysRevE.75.046303 PACS number(s): 47.27.ep, 47.90.+a

Owing to the large number of degrees of freedom involved, the equations of motion governing turbulent flows cannot, in general, be solved accurately on today's computers [1,2]. As an example, the computational cost of direct numerical simulation (DNS) of the three-dimensional Navier-Stokes equations increases as the cube of the Reynolds number, making this approach quickly impractical for high-Reynolds-number flow [1,2]. Furthermore, it is almost always the case that, in the fully resolved computations, a disproportionately high fraction of the computational effort is expended on the smaller scales whereas energy is predominantly contained in the larger scales [1,2]. Due to these considerations, further modeling is usually necessary. One of the most promising modeling techniques is large eddy simulation (LES) in which the large scale unsteady motions that are driven by the specifics of the flow geometry and forcing and that are not universal are computed explicitly and the smaller, subgrid motions (which are presumably more universal) are modeled [1–5].

In the LES technique, when the relevant governing equations are filtered to remove or reduce the energy in high-frequency modes, the resulting equations for the filtered quantities have additional terms that are thought of either as residual stresses from a purely filtering-modeling point of view (e.g., [1,2,5]) or as subgrid scale (SGS) stresses from an overall computational point of view [6]. In such a modeling strategy, when a filter is not explicitly defined, but the filtering results implicitly from the low-pass filtering characteristics of the discrete operators that use a finite stencil on the coarse grid, the resulting LES is termed implicit-filtering or grid-filtering LES [5,7]. This is by far the most commonly used form of LES.

In contrast to the implicit-filtering LES approach, of course, is the explicit-filtering LES approach wherein a filter is explicitly defined (e.g., [8]). While there are clear conceptual advantages to this latter approach, it is important to note that these advantages can be realized only when the width of the explicitly specified filter is much larger than the grid width of the LES grid [9]. This is because, if the width of the explicit filter is comparable to the grid width of the LES grid, then the previously mentioned implicit filtering effects of the discrete operator begin to be comparable to the explicit filtering. It is exactly this rather stringent requirement that makes the explicit-filtering LES approach less common among LES practitioners. Furthermore, the effects of implicit filtering are so pervasive that many authors (e.g., [1,5]) have previously stressed the need for considering its effects even when using the explicit-filtering LES approach.

A systematic study of any SGS stress model used in conjunction with the LES approach to modeling turbulence involves diagnosing the SGS stresses in appropriate fully resolved simulations. Besides the fully resolved simulations, the diagnosis of SGS stresses involves a specification of the (coarse) grid on which the LES will be performed and possibly an explicit filter [10]. While such diagnoses of SGS stresses from resolved simulations are routinely made, we wish to point out that these SGS terms may be considered from two entirely different points of view. Viewed from the point of view of the fully resolved simulations, the diagnosed SGS terms represent interactions of the large scales with the small scales and are useful in developing a physical understanding of these interactions. On the other hand, the original intent of considering the coarse mesh that is used to diagnose the SGS terms is to be able to perform an appropriate LES on that coarse mesh. Thus, viewed from the point of view of the coarser-scale simulation, the SGS terms should provide a means to achieve the same large scale dynamics in the LES as in the fully resolved simulation. If indeed the diagnosed SGS terms should provide such a means, then the diagnosed SGS terms would constitute the "perfect" subgrid model [1,7], and it is in this sense that the diagnosed SGS terms are important to the LES approach.

We show that in the context of implicit-filtering LES, the diagnosed SGS terms constitute the perfect subgrid model only under rather special circumstances. (Note that this is not related to the nonuniqueness issue of LES [11,2].) That is to say, while the original trajectory of the fully resolved simulation is realizable in the coarse-resolution simulation forced by the diagnosed SGS terms, this behavior is structurally

*Electronic address: balu@lanl.gov; URL: http://public.lanl.gov/balu
†Electronic address: livescu@lanl.gov

unstable with the perturbed trajectory falling off from the original attractor onto a different attractor all together. Thus, we demonstrate in this paper how a consideration of the issue of stability of the implicit-filtering LES with the perfect subgrid model can lead to a better understanding of both the diagnosed SGS terms and the dynamical behavior of the reduced dimensional LES.

For definiteness, we will consider a flow that is statistically stationary, although these ideas can be extended to nonstationary flows by considering ensemble averages. We will further assume that the turbulent system has a single attractor, i.e., small changes to the initial conditions of the fully resolved simulation will result in the actual trajectories diverging rapidly, but these trajectories will asymptotically lie on the same attractor. Extensive experimentation in this context (of fixed large scale forcing and other aspects of the setup) support the usual explanation that there is an instability mechanism that quickly randomizes the small scales and shows up in our diagnostic as a quick divergence of the actual trajectories. An explicit demonstration of this feature of turbulence in the three-dimensional, isotropic, and homogeneous setting is given, e.g., in Ref. [12].

Let the governing equation of such a system be a partial differential equation (PDE) of the (nondimensional) form

$$\frac{\partial q}{\partial t} = R(q), \tag{1}$$

with the usual notation. Let the above equation be computed on a fine grid to obtain a (spatially converged) finely resolved (FR) numerical solution that is representative of the solution of the above equation. Let $q^f(x,t)$ represent one such trajectory:

$$\frac{\partial q^f}{\partial t} = R(q^f). \tag{2}$$

The above equation is to be viewed as the semidiscrete form of (1) that results after spatial discretization. The additional notation in (2) is (a) that the superscript f denotes that the primary variable is discretized and resides on a "fine" grid and (b) that the discrete operator R is computed on the grid on which its argument resides, so that in the above equation $R(q^f)$ is computed on the fine grid. Note that, with the assumption of a single attractor in this system, the trajectories themselves diverge rapidly with small changes to the initial conditions, but that statistics on these perturbed trajectories remain the same.

Next, consider a coarser grid on which we wish to perform LES. Given the reduced degrees of freedom on such a coarser mesh, one can hope, in the ideal case, to reproduce only the larger scale features of the actual FR trajectory $q^f(x,t)$ that are representable on the coarser mesh. Let the image of $q^f(x,t)$ in this reduced dimensional grid space be denoted by $q^{fc}(x,t)$ where the additional superscript c stands for the coarsely resolved grid. For the physical space-grid-based numerical schemes that we are interested in (in contrast to modal schemes), the image is typically obtained as a projection and is equivalent to sampling the finer grid at the locations of the coarsely resolved grid points.[1]

Computing Eq. (1), the original governing equation, without additional modeling on this coarsely resolved grid—a bare truncation (BT)—would lead to a poorly resolved computation. Let us denote such a trajectory by $q^c_{BT}(x,t)$, where now the superscript c implies that the primary variable resides on the coarsely resolved grid. For economy of notation, we will leave out the superscript c in the rest of the paper when there is no ambiguity:

$$\frac{\partial q_{BT}}{\partial t} = R(q_{BT}). \tag{3}$$

To be sure, the discrete operator R is now computed on the grid on which q_{BT} resides, which is the coarsely resolved grid. Furthermore, it is the low-pass filtering nature of R on the coarsely resolved grid that is the source of filtering in implicit-filtering LES. Clearly, when the system is turbulent, as we have assumed, the asymptotic dynamics of the trajectory $q_{BT}(x,t)$ lie on an attractor different from the attractor of the FR simulation.

Finally, let $q_{les}(x,t) \equiv q^c_{les}(x,t)$ represent a trajectory of the LES carried out on the same coarsely-resolved mesh but with additional SGS modeling M:

$$\frac{\partial q_{les}}{\partial t} = R(q_{les}) + M. \tag{4}$$

At the risk of oversimplifying, one may state that the aim of the LES approach to modeling turbulence is to devise a model M for the effects of the SGS on the resolved scales, that would bring $q_{les}(x,t)$ closer to $q^{fc}(x,t)$ than $q_{BT}(x,t)$ already is to $q^{fc}(x,t)$, in an appropriate norm; one may demand outright closeness of the trajectories to the extent that the shape and topology of the coherent structures of the flow are

[1]With physical space discretizations like finite volume or finite difference, while the mapping from the fully resolved simulation space to the coarsely resolved LES space is most often described as a filtering process, it is more appropriate and useful to think of this mapping as a combination of a filtering operation and a projection operation. Physical space discretizations are usually thought of as related to an implicit top hat-shaped filter:

$$\tilde{g}(x) = \frac{1}{\delta^+ - \delta^-} \int_{x-\delta^+(x)}^{x+\delta^+(x)} g(x')dx'.$$

However, the top-hat filter is nearly invertible, which implies that not much information is lost. In fact the bulk of the loss of information associated with going from the fully resolved space to the LES space is indeed related to the sampling of $\tilde{g}$ on the LES grid (e.g., see [13]). It is for this reason that we emphasize the projection operator. From another point of view, the combination of the top-hat filter and the sampling on a grid produces a mapping that is more like a volume average on discrete volumes [13]. A first-order approximation of such a volume average would correspond to the mapping operation that we consider in this paper. Clearly, higher-order approximations of the volume average could be considered, but that is neither necessary nor central to the kinds of issues dealt with here.

reproduced, as may be appropriate in transient problems, or one may demand closeness in some statistical sense as may be appropriate in a statistically stationary problem [14].

The aim of this paper is not to develop or postulate a new SGS model, but rather to obtain, using the FR computation, the perfect (implicit-filtering) SGS model and to demonstrate the generic instability of the implicit-filtering LES computations that use the perfect SGS model.

To obtain the perfect SGS model, consider the image of the dynamics of the FR computation (2) in the coarsely resolved grid space:

$$\frac{\partial q^{fc}}{\partial t} = R^c(q^f). \tag{5}$$

Besides the previously defined notation, in this equation, $R^c(q^f)$ means that the discrete operator R itself is computed on the finely resolved grid, but then only its image in the coarsely resolved grid is considered. It would, however, be useful to relate the right-hand side of the above equation to $R(q^{fc})$. To this end, we define a field $D(x,t)$ as

$$D(x,t) = R^c(q^f(x,t)) - R(q^{fc}(x,t)). \tag{6}$$

Note that $D(x,t)$ is defined on the coarse mesh, and implicit in its definition is the implicit-filtering nature of the discrete operator R acting on the coarsely resolved grid in the second term. Clearly, if we considered the usual case of advective nonlinearity of fluid dynamics, $D(x,t)$ would be the divergence of the SGS stress tensor which itself consists of the Leonard stress, the cross stress, and the SGS Reynolds stress [2], but for the present purpose it suffices to consider them as a unified "eddy force" that drives the evolution of the primary variable q. Thus, we will simply call the field $D(x,t)$, the diagnosed eddy force. In terms of D, (5) may be trivially rewritten as

$$\frac{\partial q^{fc}}{\partial t} = R(q^{fc}) + D. \tag{7}$$

Comparing (4) and (7), it can now be seen that the trajectory of the LES, $q_{les}(x,t)$, would correspond exactly to the image trajectory $q^{fc}(x,t)$ of the FR simulation [i.e., $q_{les}(x,t) \equiv q^{fc}(x,t)$], if the initial conditions are identical:

$$q_{les}(x,0) = q^{fc}(x,0), \tag{8}$$

and the exact history of the diagnosed eddy force $D(x,t)$ as defined in (6) is used for the model M in Eq. (4). It is only in this very specific case that the diagnosed eddy force $D(x,t)$ will constitute the perfect SGS model. As an aside regarding the nonuniqueness of LES, note that with this procedure, if in the FR run $q^{fc}(x,0)$ were held the same and only the SGS modes were changed, $D(x,t)$ would, in general, be different and consequently we would perform a new LES.

The above discussions are completely general and do not depend on the actual form of the governing equations, but at this point we would like to consider numerical realizations of a particular flow to better demonstrate the ideas. And for this purpose, we will consider the setting of the quasigeostrophic equations describing the dynamics of wind-driven ocean circulation in the upper ocean. The quasigeostrophic equations

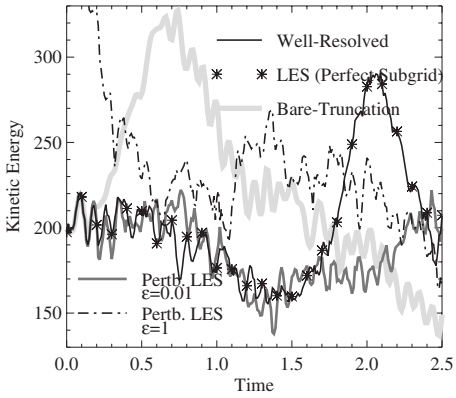

FIG. 1. Initial evolution of the (nondimensional) kinetic energy (KE). Time is in terms of eddy-turnover times. The low-resolution simulation with the perfect subgrid model identically reproduces the fully resolved solution. A small perturbation of the initial condition leads to a quick decorrelation of the low-resolution run from the fully resolved run. Also shown are the initial evolutions of KE for the case with a large perturbation of the initial condition and the bare truncation case.

themselves are a good model for describing the dynamics of large scale turbulent flows in the atmosphere and in the ocean [15]. Turbulence at these large scales is geostrophically balanced and quasi-two-dimensional in the sense of displaying an inverse cascade of energy (from small scales to large scales) [16]. Note that the direction of cascade of energy in this setting is opposite to that in three-dimensional turbulence. The code to solve the equations is described in [17], and is well tested.

We first describe a set of FR computations. The ocean model is subjected to steady forcing, and the initial spin-up phase is not considered. Note also that all the results shown for the FR computations are only with respect to the corresponding image in the reduced dimensional coarsely resolved LES grid space. Furthermore, for convenience, all results in this paper are presented in a nondimensional form, just as the governing equations were considered in a nondimensionalized form. In Fig. 1, the initial evolution of the domain integrated kinetic energy (KE) for the FR run is plotted using a thin black line. Figure 2 shows the corresponding spectra of the asymptotic long time behavior. It is clear that the system is highly unsteady and displays rich variability. Extensive previous studies have shown that, with increasing magnitude of the steady forcing, the asymptotic dynamics of the model undergoes sequences of bifurcations, ranging from the initially simple local bifurcations such as pitchfork, saddle-node, and Hopf bifurcations to later highly complicated global homoclinic bifurcations to spontaneously give rise to variability on a wide range of scales (e.g., see [18]). The time-averaged circulation stream function and potential-vorticity fields, with averaging over a period of 100 time units, are shown in Figs. 3 and 4. These fields are considered to be representative of low-order moments on the attractor. Contours with positive values of the nondimensionalized stream function and potential vorticity are drawn in continuous lines and those with negative values are drawn in broken lines in Figs. 3 and 4. Associated with positive values of the

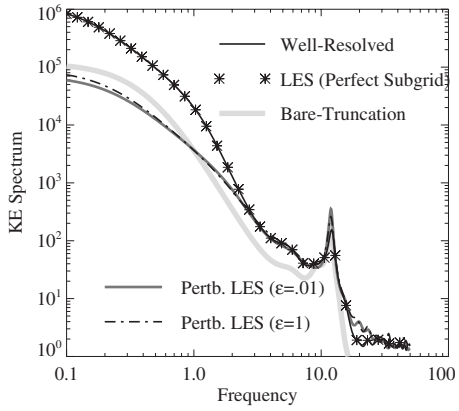

FIG. 2. (Nondimensionalized) spectra of the KE corresponding to the cases in Fig. 1. Note that the spectra for the cases with small and large perturbations of the initial condition are nearly the same. This is different from the case with no perturbations, which reproduces the spectrum of the fully resolved case. Also shown is the spectrum for the bare truncation case.

stream function are gyres in which the circulation is clockwise and vice versa. The inner gyres are in the sense of the wind forcing and may thus be called "direct" wind-driven gyres whereas the outer gyres are indirectly driven by the eddy fluxes.

We also performed two other FR runs on the fine mesh with the only difference being a random perturbation of the initial conditions according to

$$q^f_{prtb}(x,0) = q^f(x,0)[1 + \epsilon\mathcal{R}(x^f)], \tag{9}$$

where $\mathcal{R}$ is a zero-mean, unit-variance random number field that is white in space and has a Gaussian probability distribution function; the two cases correspond to small, ϵ=.01, and large, ϵ=1 perturbations. Comparing the two cases whose initial conditions differ slightly (ϵ=0 and 0.01), we

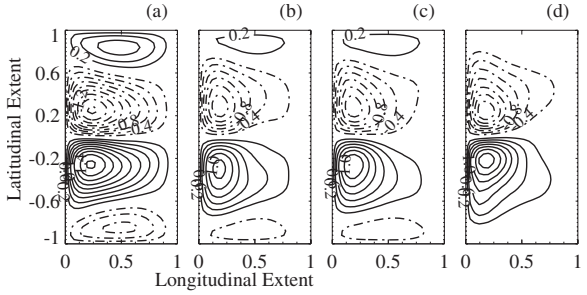

FIG. 3. Contour plots of time-mean circulation. The longitudinal and latitudinal extents are nondimensionalized and cover the full domain. Contours with positive values of the nondimensionalized stream function are drawn in continuous lines and those with negative values are drawn in broken lines. (a) corresponds to both the FR case and the perfect subgrid model case. (b), (c) are the small (large) perturbation of IC of the perfect case. (d) Bare truncation case. Differences between (b) and (c) are small compared to the differences between (a) and (b) or (c) or those between (a) and (d). The contour interval is the same in all cases and is 0.2 nondimensional stream function units.

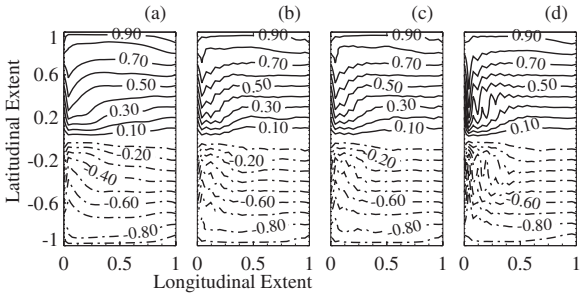

FIG. 4. Contour plots of time-mean (nondimensional) potential vorticity. Same ordering as in Fig. 3. Note that the large truncation errors in (d), the BT case (particularly evident in the western margins of the domain) are fully compensated for by the diagnosed eddy force in (a), the perfect subgrid model case, and partially reduced in cases (b) and (c) which correspond to small and large perturbations of the IC of (a). The contour interval is the same in all cases and is 0.1 nondimensional potential-vorticity units.

find that the actual trajectories diverge rapidly. However, if we consider the time-mean circulation, a low-order moment on the attractor, for each of the three cases (ϵ=0, 0.01, and 1), the differences are insignificant (figures not shown); the specifics of the initial conditions are quickly forgotten and the system "relaxes" onto the stable attractor. It is in this sense that the FR computations are robust. In terms of the diagnosed SGS term $D(x,t)$, we emphasize that the specific time histories (under perturbations) are very different, but their statistical properties are very similar.

Next, we consider a set of LES runs. We have numerically verified, in a number of cases spanning a variety of settings that $q_{les}(x,t) \equiv q^{fc}(x,t)$, when the initial conditions are identical as in Eq. (8) and when the eddy force $D(x,t)$ diagnosed as in Eq. (6) is used for M in Eq. (4). For the particular case being discussed, this is evident from the symbols corresponding to $q_{les}(x,t)$ trajectory lying identically on top of the line corresponding to the $q^{fc}(x,t)$ trajectory obtained from the FR simulation both in Fig. 1 showing the initial evolution of KE in time and in Fig. 2 showing the frequency spectra obtained from the long-time evolution of KE in the different systems. By long, here we mean times of $O(1000)$ larger than the error doubling time of the system, which itself is about 0.05 time units. We refer to this case as the perfect case.

While a diagnosis of SGS terms as in Eq. (6) have routinely been carried out, the stability of the particular solution trajectory $q_{les}(x,t)=q^{fc}(x,t)$ in the implicit-filtering LES setting of Eq. (4) when using the diagnosed eddy force $D(x,t)$ has not been investigated before. We, therefore consider two other runs performed at the coarse resolution and along with the diagnosed eddy force $D(x,t)$, as in the previous case, with the only difference being that the initial condition (IC) is randomly perturbed from that of the previous case according to

$$q_{les}(x,0) = q^{fc}(x,0)[1 + \epsilon\mathcal{R}(x)], \tag{10}$$

with ϵ=0.01 and 1, and $\mathcal{R}$ as before in Eq. (9). While it is not surprising that the trajectory of the ϵ=0.01 case diverges

quickly from the original trajectory in Fig. 1 (chaotic system), what is surprising is that the two trajectories asymptotically lie on entirely different attractors, as evident from a comparison of the corresponding time-mean circulations in Figs. 3 and 4 and the spectra of KE in Fig. 2.

Next, considering the case with the large perturbation of the initial condition ($\epsilon=1$) but otherwise the same as the perfect case, we note that while the trajectory of this case is uncorrelated to that of the case with the small perturbation (as, e.g., may be seen in Fig. 1), the differences in both the time-mean circulation and the detailed frequency spectra of the two cases are practically insignificant. This suggests that the asymptotic dynamics of the two cases ($\epsilon=0.01$ and 1) lie on the same attractor. Furthermore, this is indicative of the stability of the attractor that is sampled when the perfect LES system is perturbed. These computations therefore suggest that the attractor of the FR computations, while it can be reached in the implicit-filtering LES, is highly unstable, and that the actual attractor of the LES system that is almost always sampled is quite different from the attractor of the FR computations.

The observation that the trajectories of both the perturbed cases ($\epsilon=0.01$ and 1) lie on the same attractor (which is different from the attractor of the FR case) can be understood from the fact that the evolving states of the perturbed systems get rapidly decorrelated from the corresponding state of the unperturbed system. This in turn leads to the diagnosed eddy force field $D(x,t)$ in the perturbed cases being uncorrelated to the actual evolving state of system, making it act like an additive stochastic forcing field whose characteristics are identical in all detail to that of $D(x,t)$. The two perturbed cases ($\epsilon=0.01$ and 1) would then simply correspond to two different realizations of the additive stochastic closure, and would thus be expected to behave similarly in their long-time averages. Furthermore, the observation that the trajectories of both the perturbed cases ($\epsilon=0.01$ and 1) lie on the same attractor, but that the individual trajectories themselves are highly uncorrelated is again consistent with the loss of predictability of small scale motion in fluid turbulence demonstrated in Ref. [12].

In this context, it is also useful to consider the results from Ref. [19]. In that paper, the author considers the question of when a subgrid-scale model can yield correct statistics of the resolved fields in a LES of a turbulent flow. The author shows that while this question cannot be answered in the sense of obtaining *sufficient* conditions on the statistical properties of the modeled subgrid stress tensor, from a consideration of the filtered Navier-Stokes equations, much useful information in the form of *necessary* conditions on the statistical properties of the modeled subgrid stress tensor can be obtained (by considering increasingly higher-order moments of the filtered Navier-Stokes equations). The modeled eddy force term in the perturbed LES above ($\epsilon=0.01$ and 1) satisfied the first of the necessary conditions described in Ref. [19] (which is that the mean of the modeled eddy force has to be the same as that of the real eddy force) and thus could have rendered the right statistics of the resolved fields. However, they do not, highlighting the insufficiency of these conditions. The decorrelation argument of the previous paragraph is essentially another way of expressing the likely possibility that the modeled eddy force terms in the perturbed LES above ($\epsilon=0.01$ and 1) do not satisfy the second of the necessary conditions of Ref. [19] (which is that certain correlations between the modeled subgrid-scale stress tensor and LES field have to be the same as that between the real subgrid-scale stress tensor and the corresponding filtered turbulent fields.)

To put the comparison of Fig. 3(b) or Fig. 4(c) with Fig. 3(a) (and the corresponding comparisons in Fig. 4) in context, it is appropriate to also consider the BT case, which corresponds to M being deleted altogether from the LES computation. For this run, the initial evolution of KE is shown in Fig. 1, the spectrum of KE in Fig. 2, the time-mean circulation in Fig. 3(d), and the time-mean potential-vorticity in Fig. 4(d). The large differences between the BT and FR cases in Figs. 2–4 suggest, as expected, that the asymptotic dynamics of the BT case lie on an attractor different from that corresponding to the FR case.

The BT computations are useful from another point of view: Since truncation errors are significant at the coarse resolutions employed in LES, the PDE satisfied by the numerical solution of Eq. (4) may be more appropriately written as

$$\frac{\partial q_{les}}{\partial t} = R(q_{les}) + M + M^h, \tag{11}$$

where M^h is a representation of the spatial truncation error. From the large amplitude grid-scale oscillations in the long-time mean of the primary prognostic variable, potential vorticity, in Fig. 4(d) it is clear that the coarsely resolved LES grid is so coarse that numerical truncation errors are significant. So, in the BT case, M^h is large and by construction, $M=0$.

It is also evident from Fig. 4(a) that these truncation errors are absent in the perfect case, implying that the specific truncation errors of Fig. 4(d), M^h, have been compensated for via one component of the diagnosed eddy force term $D(x,t)$, denoted by D^h [in the presence of the rest of $D(x,t)$, denoted by D^r of course], through the perfect preservation of the correlation between the state of the system and $D(x,t)$.

The passage from BT [thick light lines in Figs. 1, 2, 3(d), and 4(d)] to the perfect subgrid case [asterisk in Figs. 1, 2, 3(a), and 4(a)] is better seen qualitatively as two separate steps: In the first step D^r acts on BT to bring it to the perturbed case [either of the two Pertb. LES cases in Figs. 1, 2, 3(b), and 4(b) or Figs. 3(c) and 4(c)] and in the second step D^h perfectly compensates for the reduced truncation error of the perturbed case. In the perturbed cases ($\epsilon=0.01$, and 1) themselves, the correlation between $D(x,t)$ and the state of the system having been derailed through perturbations of the initial conditions, the second step is unable to compensate for the (now partly reduced) truncation error. So the grid-scale oscillations in the potential-vorticity field persist at the reduced level in the perturbed cases [Figs. 4(b) and 4(c)]. In this context, the component D^r can be thought of as one optimal estimate of the subgrid eddy force in the sense of Langford and Moser [13]. Thus the differences between the perturbed LES and FR simulations above are likely related to

the limit on the achievable accuracy of LES due to the loss of information incurred in the filtering process.

Implicit in this argument is the reasoning that the improved circulation in the $\epsilon=0.01$ and 1 cases as compared to the bare truncation case is indicative of the beneficial effects of the additive stochastic closure here. This is a subject of ongoing research and we will report it elsewhere. (Furthermore, given the vastly differing nature of scale interactions in two-dimensional and three-dimensional turbulence, we plan to investigate the usefulness of an additive stochastic closure separately in the three-dimensional context.) Nevertheless, the fact that the grid-scale oscillations have been reduced in the $\epsilon=0.01$ and 1 cases as compared to the bare truncation case is consistent with the reduced resolution requirement in the presence of this closure. It is interesting to consider the case of driving M^h to 0 while keeping resolution coarse of course, as for example, by using an adaptive implicit viscosity on the lines of implicit LES (ILES) [20]. Some computations we have performed using one such ILES approach did not lead to the time-mean circulation approaching that for the FR or perturbed LES cases [21], although as mentioned earlier, it eliminates truncation errors that lead to grid-scale oscillations in the time-mean potential-vorticity field. These computations, thus reiterate the importance of interpreting the diagnosed SGS terms in a combined physical-numerical setting rather than in a purely physical or purely numerical setting.

Funding for this work was provided in part by the LDRD program office at LANL under Grant No. 20050066DR and in part by the DOE CCPP component at LANL.

[1] B. J. Geurts, *Elements of Direct and Large-Eddy Simulation* (Edwards, Philadelphia, 2004).
[2] S. B. Pope, *Turbulent Flows* (Cambridge University Press, Cambridge, U.K., 2000), Chap. 13.
[3] P. Givi, Prog. Energy Combust. Sci. **15**, 1 (1989).
[4] C. Meneveau and J. Katz, Annu. Rev. Fluid Mech. **32**, 1 (2000).
[5] G. De Stefano and O. V. Vasilyev, Theor. Comput. Fluid Dyn. **18**, 27 (2004).
[6] S. B. Pope, New J. Phys. **6**, 1 (2004).
[7] G. De Stefano and O. V. Vasilyev, Phys. Fluids **14**, 362 (2002).
[8] G. S. Winckelmans, A. A. Wray, O. V. Vasilyev, and H. Jeanmart, Phys. Fluids **13**, 1385 (2001).
[9] B. J. Geurts and J. Frolich, Phys. Fluids **14**, L41 (2002).
[10] A. Leonard, Adv. Geophys. **A18**, 237 (1974).
[11] J. L. Guermond, J. T. Oden, and S. Prudhomme, J. Math. Fluid Mech. **6**, 194 (2004).
[12] L. Machiels, Phys. Rev. Lett. **79**, 3411 (1997).
[13] J. A. Langford and R. D. Moser, J. Fluid Mech. **398**, 321 (1999).
[14] M. Lesieur, *Turbulence of Fluids*, 3rd ed. (Kluwer Academic, Dordrecht, 1997), Chap. 12, pp. 375–408.
[15] G. K. Vallis, *Atmospheric and Oceanic Fluid Dynamics* (Cambridge University Press, Cambridge, U.K., 2006).
[16] R. H. Kraichnan, Phys. Fluids **10**, 1417 (1967).
[17] R. J. Greatbatch and B. T. Nadiga, J. Phys. Oceanogr. **30**, 1461 (2000).
[18] B. T. Nadiga and B. Luce, J. Phys. Oceanogr. **31**, 2669 (2001).
[19] C. Meneveau, Phys. Fluids **6**, 815 (1994).
[20] L. G. Margolin, W. J. Rider, and F. F. Grinstein, J. Turbul. **7**, 1 (2006).
[21] B. T. Nadiga, Los Alamos Report No. LA-UR-06-7647, 2006 (unpublished).